

Article

# High-Voltage Polyanion Positive Electrode Materials

Atsuo Yamada

Department of Chemical System Engineering, The University of Tokyo, Tokyo 113-8656, Japan;  
yamadal@chemsys.t.u-tokyo.ac.jp

**Abstract:** High-voltage generation (over 4 V versus  $\text{Li}^+/\text{Li}$ ) of polyanion-positive electrode materials is usually achieved by  $\text{Ni}^{3+}/\text{Ni}^{2+}$ ,  $\text{Co}^{3+}/\text{Co}^{2+}$ , or  $\text{V}^{4+}/\text{V}^{3+}$  redox couples, all of which, however, encounter cost and toxicity issues. In this short review, our recent efforts to utilize alternative abundant and less toxic  $\text{Fe}^{3+}/\text{Fe}^{2+}$  and  $\text{Cr}^{4+}/\text{Cr}^{3+}$  redox couples are summarized. Most successful examples are alluaudite  $\text{Na}_2\text{Fe}_2(\text{SO}_4)_3$  (3.8 V versus sodium and hence 4.1 V versus lithium) and  $\beta_1\text{-Na}_3\text{Al}_2(\text{PO}_4)_2\text{F}_3$ -type  $\text{Na}_3\text{Cr}_2(\text{PO}_4)_2\text{F}_3$  (4.7 V versus sodium and hence 5.0 V versus lithium), where maximizing  $\Delta G$  by edge-sharing  $\text{Fe}^{3+}\text{-Fe}^{3+}$  Coulombic repulsion and the use of the  $3d^2/3d^3$  configuration of  $\text{Cr}^{4+}/\text{Cr}^{3+}$  are essential for each case. Possible exploration of new high-voltage cathode materials is also discussed.

**Keywords:** cathode; polyanion; high-voltage



**Citation:** Yamada, A. High-Voltage Polyanion Positive Electrode Materials. *Molecules* **2021**, *26*, 5143. <https://doi.org/10.3390/molecules26175143>

Academic Editors: Stephane Jobic, Claude Delmas and Myung-Hwan Whangbo

Received: 21 July 2021

Accepted: 21 August 2021

Published: 25 August 2021

**Publisher's Note:** MDPI stays neutral with regard to jurisdictional claims in published maps and institutional affiliations.



**Copyright:** © 2021 by the author. Licensee MDPI, Basel, Switzerland. This article is an open access article distributed under the terms and conditions of the Creative Commons Attribution (CC BY) license (<https://creativecommons.org/licenses/by/4.0/>).

## 1. Introduction

Polyanion-positive electrode material for lithium batteries was identified by Delmas, Goodenough, and their co-workers for the NASICON  $\text{M}_2(\text{XO}_4)_3$  framework in the 1980s [1–3]. Later on, Padhi, Nanjundaswamy, and Goodenough discovered a very promising positive electrode material,  $\text{LiFePO}_4$  [4], which is now widely commercialized for stationary use or a power source for electric vehicles. A common advantage of polyanion-type electrodes is their long-term stability of operation due to the rigid structural framework. Additional advantages inherent to  $\text{LiFePO}_4$  that have led to its commercial application are (i) lithium can be extracted at the first charge and functions as a charge carrier, moving back and forward upon charge/discharge, (ii) it can withstand self-decomposition to guarantee a high level of safety, and (iii) it has a suitable operating voltage of 3.4 V versus lithium, which is not so high that it decomposes electrolytes but not too low that energy density is sacrificed [5].

Toward higher voltages, Mn analogue  $\text{LiMnPO}_4$  (4.1 V versus lithium) was investigated but its low electrochemical activity was not acceptable, and this negative feature is common for all Mn-based polyanion-positive electrode materials [4,6–8]. Vanadium-based compounds such as  $\text{LiVPO}_4\text{F}$  [9] operate well at a reasonable voltage range around 4.2 V, but they have been excluded as a commercial option due to the element's toxicity and the volume change during  $\text{Li}^+$  de/intercalation [10,11]. For an even higher voltage,  $\text{Co}^{3+}/\text{Co}^{2+}$  and  $\text{Ni}^{3+}/\text{Ni}^{2+}$  redox couples show activity at  $>4.5$  V [12–14], but their highly oxidizing nature induces several side reactions unless careful design is applied to both the electrolyte and electrode composite. For a sodium analogue, electrode operation at higher voltages is more important as the  $\text{Na}/\text{Na}^+$  potential is ca. 0.3 V higher than the  $\text{Li}/\text{Li}^+$  potential. Within the polyanionic materials, strategic design toward high-voltage operation is almost the same in the case of lithium, achieved by introducing V, Co, Ni as a redox center, as represented by  $\text{Na}_4\text{Co}_3(\text{PO}_4)_2\text{P}_2\text{O}_7$  [15–17].

However, the use of V, Co, or Ni is a challenging option for battery engineers as they entail cost and toxicity issues. In particular, for a sodium battery system, a high-voltage system with more abundant and cheap elements would be ideal. In this short review article, after summarizing the influential factors dominating positive electrode

voltage, our recent successful attempts to activate  $\text{Fe}^{3+}/\text{Fe}^{2+}$  and  $\text{Cr}^{4+}/\text{Cr}^{3+}$  redox couples, in  $\text{Na}_2\text{Fe}_2(\text{SO}_4)_3$  (3.8 V versus sodium and hence 4.1 V versus lithium) [18] and  $\beta_1\text{-Na}_3\text{Al}_2(\text{PO}_4)_2\text{F}_3$ -type  $\text{Na}_3\text{Cr}_2(\text{PO}_4)_2\text{F}_3$  (4.7 V versus sodium and hence 5.0 V versus lithium) [19], will be demonstrated.

## 2. Toward Higher Voltage

### 2.1. Inductive Effect in Polyanionic Compounds

The voltage trend of polyanion-based positive electrode materials roughly follows the formal charges of the central atoms in the polyanions, consisting of the idea of the inductive effect [20]. The presence of strong X-O covalency stabilizes the antibonding  $M^{3+}/M^{2+}$  state through an M-O-X inductive effect to generate an appropriately high voltage. A series of compounds including large polyanions  $(\text{XO}_4)^{y-}$  ( $X = \text{S, P, As, Mo, W, } y = 2 \text{ or } 3$ ) were explored, and the use of  $(\text{PO}_4)^{3-}$  and  $(\text{SO}_4)^{2-}$  has been shown to stabilize the structure and lower the  $M^{3+}/M^{2+}$  redox energy to useful levels.

### 2.2. Thermodynamic Modification

In essence, the voltage is defined as the difference between the lithium chemical potential in the cathode and in the anode, leading to a simple thermodynamic definition, ignoring  $PV$  and  $TS$  terms: ( $P = \text{pressure, } V = \text{volume, } T = \text{temperature, and } S = \text{entropy}$ ),  $E = (G_{\text{Li}} + G_{\text{charged}} - G_{\text{discharged}})/nF$ , where  $G_{\text{Li}}$ ,  $G_{\text{charged}}$ , and  $G_{\text{discharged}}$ , are the Gibbs free energies of lithium metal, charged cathode, and discharged cathode, respectively;  $n$  is the number of electrons in the redox reaction, and  $F$  is the Faraday constant. The overall thermodynamic scheme for voltage generation is summarized in Figure 1 based on the Born–Haber cycle [21].

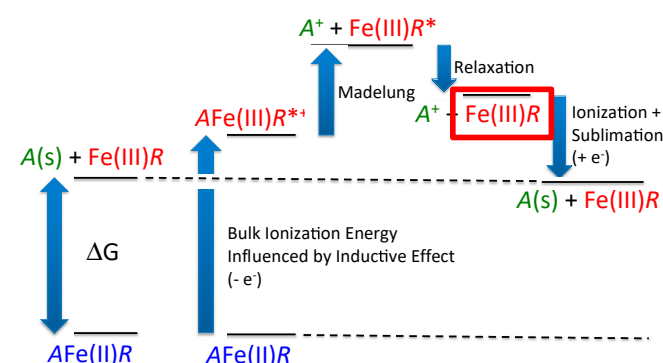


**Figure 1.** A Born–Haber cycle for the definition of voltage generation in cathode materials based on  $\text{Fe}^{3+}/\text{Fe}^{2+}$  redox couple. The notations  $R$  and  $R^*$  represent relaxed and unrelaxed frameworks, respectively. Bulk ionization energy, which is closely related to the inductive effect, is an approximation (electronic part) but is not identical to  $\Delta G$ .

### 2.3. Choice of Transition Metals

Figure 2 shows a schematic derivation of the operation voltages and  $d$ -band positions of  $3d$  transition metal phosphates in sodium ion batteries. [19] In general, a transition metal ion  $M^{n+}$  with a higher atomic number has a deeper valence level owing to a larger effective nuclear charge, resulting in a higher  $M^{(n+1)+}/M^{n+}$  redox potential. Naturally, phosphates with end representatives of the  $3d$  series, such as  $\text{Co}^{2+}$  and  $\text{Ni}^{2+}$ , typically  $\text{Na}_2\text{CoPO}_4\text{F}$  and  $\text{Na}_4\text{M}_3(\text{PO}_4)_2\text{P}_2\text{O}_7$  ( $M = \text{Co}^{2+}$  and  $\text{Ni}^{2+}$ ), have been reported as high-voltage (4.3 V, 4.4 V, 4.8 V, respectively) cathode materials [16,17,22–24]. However, end representatives of the  $3d$  series suffer from energy-level increments either by spin exchange penalty or crystal field splitting. On the other hand, the  $3d^3$  electron of  $\text{Cr}^{3+}$  in the  $t_{2g}$  orbital is free from both spin exchange and crystal field splitting, which can be compensated for the smaller nuclear charge. Indeed,  $\text{Cr}^{4+}/\text{Cr}^{3+}$  redox couples in phosphates generate  $>4.5$  V vs.  $\text{Na}/\text{Na}^+$  (as presented below) [19], comparable to Co- or Ni-based phosphates.

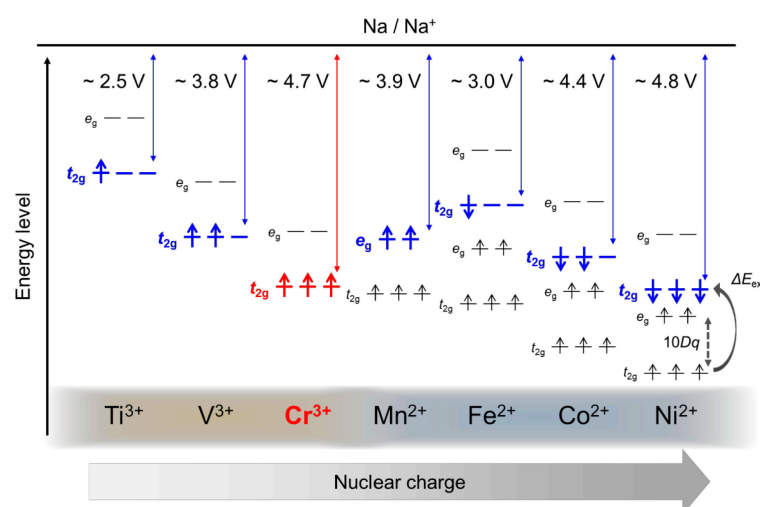


**Figure 2.** Schematic comparison of operating voltages and d-electron configurations for phosphate-based cathode materials containing 3d transition metals [19].  $10Dq$  and  $\Delta E_{ex}$  indicate an octahedral crystal field splitting energy for 3d orbitals and exchange splitting energy, respectively. Orange and blue shading corresponds to valences of 3 and 2, respectively. Note that there is also a contribution of the Madelung and other energies to the cell voltage that is superimposed on the electronic contribution of the transition metal ions (see Figure 1). Permission is granted by Chemistry of Materials.

### 3. High-Voltage System with $\text{Fe}^{3+}/\text{Fe}^{2+}$ and $\text{Cr}^{4+}/\text{Cr}^{3+}$

#### 3.1. Pyrophosphates

Of particular interest is the triplite phase of  $\text{LiFeSO}_4\text{F}$  [25] and metal-doped  $\text{Li}_2\text{FeP}_2\text{O}_7$  [26,27] possess edge-sharing  $\text{FeO}_6$  octahedra to minimize the Fe-Fe distance, as distinguished from other, lower-voltage Fe-based polyanion electrodes with corner-sharing octahedra. A shorter  $\text{Fe}^{3+}\text{-Fe}^{3+}$  distance in the charged state is effective for enlarging  $G_{\text{charged}}$ , and hence the operating voltage  $E$ , while the influence of the discharged state  $G_{\text{discharged}}$  with smaller charge  $\text{Fe}^{2+}$  can be subordinated in energetics.

The cell voltage for these two materials can reach as high as 3.9 V (vs. Li), which is higher than the value of 3.8 V calculated from the standard redox potentials. The latter has been suggested to be the highest achievable voltage for a Li ion battery utilizing the  $\text{Fe}^{3+}/\text{Fe}^{2+}$  redox couple in solid. As shown in Figure 3, the potential tunability for the  $\text{Fe}^{3+}/\text{Fe}^{2+}$  redox couple at the unusually high-voltage region of 3.5–3.9 V vs. lithium is similar for any metal  $M$  doping in the  $\text{Li}_2M_x\text{Fe}_{1-x}\text{P}_2\text{O}_7$  system [27]. The phenomena include two aspects: (1) two redox reactions at different potentials are stabilized with the doping of foreign metal  $M$ , (2) with more dopant, both of the redox reactions upshift to higher potential, and one even approaches 4 V. Substitution of  $M$  into Fe sites may suppress the migration of Fe from the  $\text{FeO}_5$  site upon charging, and the two original, distinct Fe sites become robust to stabilize the edge-sharing geometry of  $\text{FeO}_5$  and  $\text{FeO}_6$  polyhedrals with large  $\text{Fe}^{3+}\text{-Fe}^{3+}$  coulombic repulsion energy, leading to the two distinct redox reactions with inherently high potentials. The change in the relative energy of the intermediate compounds, which is induced by the unfavorable  $V_{\text{Li}}' - M^{2+}(M_{\text{Fe}}^\times)$  and/or  $\text{Li}_{\text{Li}}^\times - \text{Fe}^{3+}(\text{Fe}_{\text{Fe}}^\bullet)$  interaction in the doping case, may be a reason for the further potential upshifting. The classic inductive effect cannot explain the redox potential upshifting phenomenon in this case.

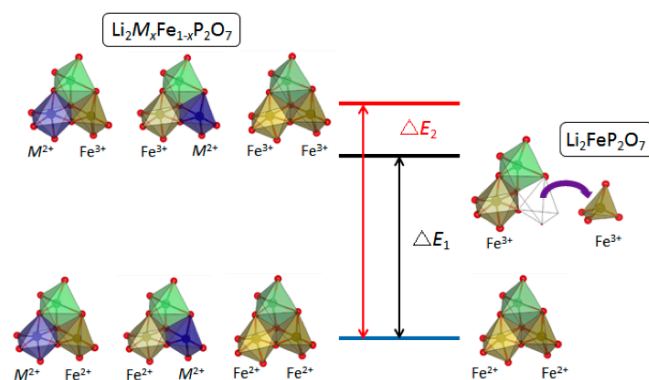


**Figure 3.** Schematic description of free energy difference between starting and delithiation materials. The right-hand portion is the pristine  $\text{Li}_2\text{FeP}_2\text{O}_7$  system. The spontaneous structural rearrangement (Fe's migration) destroys the edge-sharing configuration and decreases the free energy of the delithiated state, which results in an energy difference of  $\Delta E_1$ . The left-hand portion is the doping system  $\text{Li}_2\text{M}_x\text{Fe}_{1-x}\text{P}_2\text{O}_7$ . After full delithiation, the Li concentration is higher than that in the  $\text{Li}_2\text{FeP}_2\text{O}_7$  case, because all of the  $M$  ions remain inert. The remaining Li can block the Fe migration and can stabilize the Fe's original local structure and the whole crystal structure, which means that the energy difference  $\Delta E_2$  should be higher than  $\Delta E_1$ .

### 3.2. Alluaudites

Compaction of the  $\text{MO}_6$  dimer can be more pronounced in an alluaudite framework, where two edge-shared  $\text{MO}_6$  octahedra are bridged by a small  $\text{XO}_4$  tetrahedron and the  $M$ - $M$  distance becomes much shorter (Figure 4). During the search along the  $\text{Na}_2\text{SO}_4$ - $\text{FeSO}_4$  tie line, we discovered the first sulfate compound with an alluaudite-type framework [18]. Deviating sharply from most of the  $A_x\text{M}_2(\text{XO}_4)_3$ -type compounds adopting the NASICON-related structures,  $\text{Na}_2\text{Fe}_2(\text{SO}_4)_3$  does not contain the lantern units  $[\text{M}_2(\text{XO}_4)_3]$ . It would be convenient to denote  $A A' B \text{M}_2(\text{XO}_4)_3$  as general alluaudite-type compounds, where  $A$  = partially occupied Na(2),  $A'$  = partially occupied Na(3),  $B$  = Na(1),  $M$  =  $\text{Fe}^{2+}$ , and  $X$  = S in the present case.

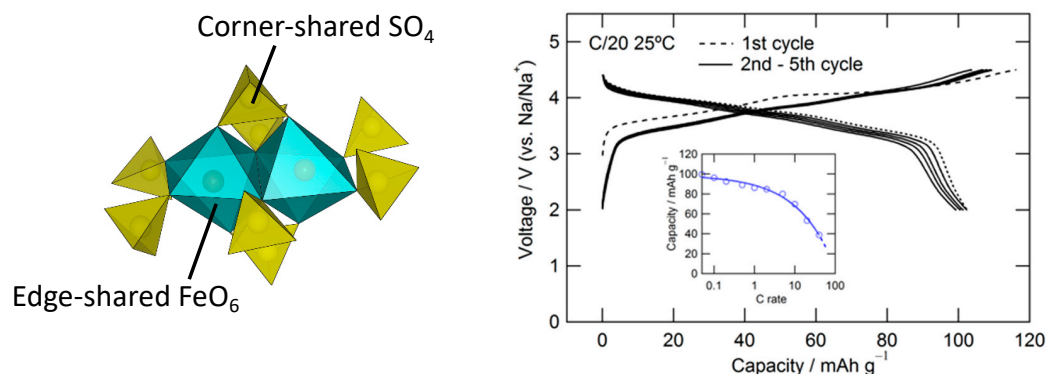


**Figure 4.** Local coordination structure and charge–discharge voltage profile of  $\text{Na}_2\text{Fe}_2(\text{SO}_4)_3$ .

The  $\text{Na}_2\text{Fe}_2(\text{SO}_4)_3$  offers an average potential of 3.8 V (vs.  $\text{Na}/\text{Na}^+$ ), with smooth, sloping charge–discharge profiles over a narrow voltage range of 3.3–4.3 V, which is the highest  $\text{Fe}^{3+}/\text{Fe}^{2+}$  redox potential obtained in any material environment (Figure 5) [18]. The abnormally high voltage can be explained by the thermodynamic definition of voltage explained in Section 2.2; the edge-sharing geometry of the Fe octahedra in  $\text{Na}_2\text{Fe}_2(\text{SO}_4)_3$  will raise  $G_{\text{charged}}$  due to the strong  $\text{Fe}^{3+}$ – $\text{Fe}^{3+}$  repulsion, leading to high  $E$ . Additionally, it offers excellent rate kinetics and cycling stability without requiring any additional cathode optimization. It forms an open framework host for the efficient (de)intercalation of Na ions with very low activation energy.

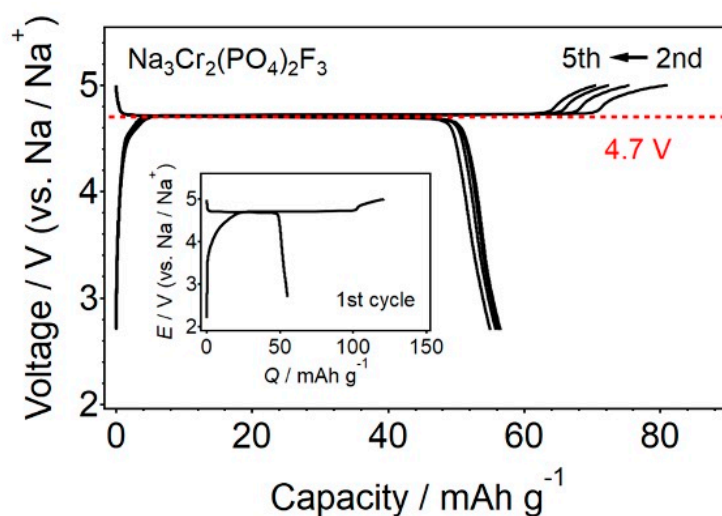


**Figure 5.** Galvanostatic charge–discharge curves of  $\text{Na}_3\text{Cr}_2(\text{PO}_4)_2\text{F}_3$  electrode in Na half-cell at a rate of 0.1 C between 2.7 and 5.0 V vs.  $\text{Na}/\text{Na}^+$  (1 C =  $63.8 \text{ mA g}^{-1}$ ). Inset shows the first cycle.

An remarkable feature is that, now, the most commonly accessible redox  $\text{Fe}^{3+}/\text{Fe}^{2+}$  can, in principle, generate the high voltage of 3.8 V vs. sodium (and hence 4.1 V vs. lithium). However, the hygroscopicity of the sulphate compounds must be carefully managed.

### 3.3. $\beta_1\text{-Na}_3\text{Al}_2(\text{PO}_4)_2\text{F}_3$ -Type Fluoride Phosphates

Considering the d-level considerations in Section 2.3, an extremely high operating potential of 4.7 V vs.  $\text{Na}/\text{Na}^+$  was identified in  $\text{Na}_{3-x}\text{Cr}_2(\text{PO}_4)_2\text{F}_3$  ( $0 < x < 1$ ) on account of the  $\text{Cr}^{4+}/\text{Cr}^{3+}$  ( $3d^2/3d^3$ ) redox couple, providing a promising design strategy for a high-voltage positive electrode material [19]. Whilst further  $\text{Na}^+$  extraction ( $x > 1$ ) to form  $\text{NaCr}_2(\text{PO}_4)_2\text{F}_3$  above 5.0 V vs.  $\text{Na}/\text{Na}^+$  remains elusive, optimization of the durable cell components for high-voltage operation may enable more activity and greater reversibility. Overall, utilizing low-cost  $\text{Cr}^{4+}/\text{Cr}^{3+}$  ( $3d^2/3d^3$ ), instead of  $\text{Co}^{3+}/\text{Co}^{2+}$  ( $3d^6/3d^7$ ) or  $\text{Ni}^{3+}/\text{Ni}^{2+}$  ( $3d^7/3d^8$ ) as in previously reported polyanion compounds, is worthwhile for the realization of batteries with higher energy density.

## 4. Summary and Perspective

Initiated by Delmas, Goodenough, and co-workers in the 1980s, polyanion-type positive electrode materials now represent a large group of materials for reversible  $\text{Li}^+$ ,  $\text{Na}^+$ , and  $\text{K}^+$  insertion. With a suitable combination of transition metal and framework structure, the operating voltage can be tuned, leading sometimes to a suitable high-voltage range for practical application. Although  $\text{LiFePO}_4$  is the only compound that has been widely applied for commercial use to date, continuous exploration is ongoing in the community toward better batteries with lower cost, high voltage, high safety, and a long calendar life. In addition to the widely examined redox couple based on  $\text{Fe}^{3+}/\text{Fe}^{2+}$ ,  $\text{Cr}^{4+}/\text{Cr}^{3+}$  could be an inexpensive yet higher-voltage option for future material development in polyanion compounds.

**Funding:** This research was funded by Element Strategy Initiative of MEXT, Grant Number JP-MXP0112101003.

**Conflicts of Interest:** The author declares no conflict of interest.

**Sample Availability:** Samples are not available without a certain contract.

## References

1. Nadiri, A.; Delmas, C.; Salmon, R.; Hagenmuller, P. Chemical and electrochemical alkali metal intercalation in the 3D framework of  $\text{Fe}_2(\text{MoO}_4)_3$ . *Rev. Chim. Minérale* **1984**, *21*, 537–544.
2. Manthiram, A.; Goodenough, J.B. Lithium insertion into  $\text{Fe}_2(\text{MO}_4)_3$  frameworks: Comparison of  $\text{M} = \text{W}$  with  $\text{M}$ . *J. Solid State Chem.* **1987**, *71*, 349–360. [[CrossRef](#)]
3. Delmas, C.; Cherkaoui, F.; Nadiri, A.; Hagenmuller, P. A Nasicon-type phase as intercalation electrode:  $\text{NaTi}_2(\text{PO}_4)_3$ . *Mat. Res. Bull.* **1987**, *22*, 631–639. [[CrossRef](#)]
4. Padhi, A.K.; Nanjundaswamy, K.S.; Goodenough, J.B. Phospho-olivines as positive-electrode materials for rechargeable lithium batteries. *J. Electrochem. Soc.* **1997**, *144*, 1188–1194. [[CrossRef](#)]
5. Yamada, A.; Chung, S.-C.; Hinokuma, K. Optimized  $\text{LiFePO}_4$  for lithium battery cathodes. *J. Electrochem. Soc.* **2001**, *148*, A224–A229. [[CrossRef](#)]
6. Yonemura, M.; Yamada, A.; Takei, Y.; Sonoyama, N.; Kanno, R. Comparative kinetic study of olivine  $\text{Li}_x\text{MPO}_4$  ( $\text{M} = \text{Fe}, \text{Mn}$ ). *J. Electrochem. Soc.* **2004**, *151*, A1352–A1356. [[CrossRef](#)]
7. Delacourt, C.; Laffont, L.; Bouchet, R.; Wurm, C.; Leriche, J.-B.; Morcrette, M.; Tarasco, J.-M.; Masquelier, C. Toward understanding of electrical limitations (electronic, ionic) in  $\text{LiMPO}_4$  ( $\text{M} = \text{Fe}, \text{Mn}$ ) electrode materials. *J. Electrochem. Soc.* **2005**, *152*, A913–A921. [[CrossRef](#)]
8. Yamada, A.; Takei, Y.; Koizumi, H.; Sonoyama, N.; Kanno, R.; Ito, K.; Yonemura, M.; Kamiyama, T. Electrochemical, magnetic, and structural investigation of the  $\text{Li}_x(\text{Mn}_y\text{Fe}_{1-y})\text{PO}_4$  olivine phases. *Chem. Mater.* **2006**, *18*, 804–813. [[CrossRef](#)]
9. Barker, J.; Saidi, M.Y.; Swoyer, J.L. Lithium Iron(II) Phospho-olivines prepared by a novel carbothermal reduction method. *Electrochem. Solid State Lett.* **2003**, *6*, A53–A55. [[CrossRef](#)]
10. Ellis, B.L.; Ramesh, T.N.; Davis, L.J.M.; Goward, G.R.; Nazar, L.F. Structure and electrochemistry of two-electron redox couples in lithium metal fluorophosphates based on theavorite structure. *Chem. Mater.* **2011**, *23*, 5138–5148. [[CrossRef](#)]
11. Chayambuka, K.; Mulder, G.; Danilov, D.L.; Notten, P.H.L. From Li-ion batteries toward Na-ion chemistries: Challenges and opportunities. *Adv. Energy Mater.* **2020**, *10*, 1–11. [[CrossRef](#)]
12. Amine, K.; Yasuda, H.; Yamachi, M. Olivine  $\text{LiCoPO}_4$  as 4.8 V electrode material for lithium batteries. *Electrochem. Solid State Lett.* **2000**, *3*, 178–179. [[CrossRef](#)]
13. Wolfenstine, J.; Allen, J.  $\text{Ni}^{3+}/\text{Ni}^{2+}$  redox potential in  $\text{LiNiPO}_4$ . *J. Power Sources* **2005**, *142*, 389–390. [[CrossRef](#)]
14. Masquelier, C.; Croguennec, L. Polyanionic (phosphates, silicates, sulfates) frameworks as electrode materials for rechargeable Li (or Na) batteries. *J. Am. Chem. Soc.* **2013**, *113*, 6552–6591.
15. Bianchini, M.; Fauth, F.; Brisset, N.; Weill, F.; Suard, E.; Masquelier, C.; Croguennec, L. Comprehensive investigation of the  $\text{Na}_3\text{V}_2(\text{PO}_4)_2\text{F}_3$ – $\text{NaV}_2(\text{PO}_4)_2\text{F}_3$  system by operando high resolution synchrotron X-ray diffraction. *J. Am. Chem. Soc.* **2015**, *27*, 3009–3020. [[CrossRef](#)]
16. Nose, M.; Nakayama, H.; Nobuhara, K.; Yamaguchi, H.; Nakanishi, S.; Iba, H.  $\text{Na}_4\text{Co}_3(\text{PO}_4)_2\text{P}_2\text{O}_7$ : A novel storage material for sodium-ion batteries. *J. Power Sources* **2013**, *234*, 175–179. [[CrossRef](#)]
17. Gezović, A.; Vujković, M.J.; Milović, M.; Grudić, V.; Dominko, R.; Mentus, S. Recent developments of  $\text{Na}_4\text{M}_3(\text{PO}_4)_2(\text{P}_2\text{O}_7)$  as the cathode material for alkaline-ion rechargeable batteries: Challenges and outlook. *Energy Storage Mater.* **2021**, *37*, 243–273. [[CrossRef](#)]
18. Barpanda, P.; Oyama, G.; Nishimura, S.; Chung, S.-C.; Yamada, A. A 3.8-V earth-abundant sodium battery electrode. *Nat. Commun.* **2014**, *5*, 1–6. [[CrossRef](#)]
19. Kawai, K.; Asakura, D.; Nishimura, S.; Yamada, A. 4.7 V Operation of the  $\text{Cr}^{4+}/\text{Cr}^{3+}$  redox couple in  $\text{Na}_3\text{Cr}_2(\text{PO}_4)_2\text{F}_3$ . *Chem. Mater.* **2021**, *33*, 1373–1379. [[CrossRef](#)]
20. Padhi, A.K.; Nanjundaswamy, K.S.; Masquelier, C.; Okada, S.; Goodenough, J.B. Effect of structure on the  $\text{Fe}^{3+}/\text{Fe}^{2+}$  redox couple in iron phosphates. *J. Electrochem. Soc.* **1997**, *144*, 1609–1613. [[CrossRef](#)]
21. Yamada, A. Systematic studies on “abundant” battery materials: Identification and reaction mechanisms. *Electrochemistry* **2016**, *84*, 654–661. [[CrossRef](#)]
22. You, Y.; Manthiram, A. Progress in high-voltage cathode materials for rechargeable sodium-ion batteries. *Adv. Energy Mater.* **2018**, *8*, 1701785. [[CrossRef](#)]
23. Chayambuka, K.; Mulder, G.; Danilov, D.L.; Notten, P.H.L. Sodium-ion battery materials and electrochemical properties reviewed. *Adv. Energy Mater.* **2018**, *8*, 1–49. [[CrossRef](#)]
24. Kubota, K.; Yokoh, K.; Yabuuchi, N.; Komaba, S.  $\text{Na}_2\text{CoPO}_4\text{F}$  as a high-voltage electrode material for Na-ion batteries. *Electrochemistry* **2014**, *82*, 909–911. [[CrossRef](#)]
25. Barpanda, P.; Ati, M.; Melot, B.; Rouse, G. A 3.90V iron-based fluorosulphate material for lithium-ion batteries crystallizing in the triplite structure. *Nat. Mater.* **2011**, *10*, 772–779. [[CrossRef](#)] [[PubMed](#)]
26. Furuta, N.; Nishimura, S.; Barpanda, P.; Yamada, A.  $\text{Fe}^{3+}/\text{Fe}^{2+}$  redox couple approaching 4 V in  $\text{Li}_{2-x}(\text{Fe}_{1-y}\text{Mn}_y)\text{P}_2\text{O}_7$  pyrophosphate cathodes. *Chem. Mater.* **2012**, *24*, 1055–1061. [[CrossRef](#)]
27. Ye, T.; Barpanda, P.; Nishimura, S.; Furuta, N.; Chung, S.-C.; Yamada, A. General observation of  $\text{Fe}^{3+}/\text{Fe}^{2+}$  redox couple close to 4 V in partially substituted  $\text{Li}_2\text{FeP}_2\text{O}_7$  pyrophosphate solid-solution cathodes. *Chem. Mater.* **2013**, *25*, 3623–3629. [[CrossRef](#)]